Multimode Free Space Optical Link Enabled by SiP Integrated Meshes

Maziyar Milanizadeh[1], SeyedMohammad SeyedinNavadeh[1],Giorgia Benci[1], Christian De Vita[1] , Charalambos Klitis[2], Marc Sorel[2], Francesco Zanetto[1], Giorgio Ferrari[1], David A.B. Miller[3], Andrea Melloni[1], Francesco Morichetti[1]

[1] Dipartimento di Elettronica, Informazione e Bioingegneria - Politecnico di Milano, Milano, 20133 Italy. (*maziyar.milanizadeh@polimi.it*)

[2] School of Engineering University of Glasgow, Glasgow, G12 8QQ, U.K

[3] Ginzton Laboratory, Stanford University, Spilker Building, Stanford, CA 94305, USA

Abstract *A silicon photonic mesh of tuneable Mach-Zehnder Interferometers (MZIs) is employed to receive two spatially-overlapped Hermite-Gaussian beams modulated at 10 Gbit/s, sharing the same wavelength and state of polarization. The mesh automatically self-configures, separating and sorting the two beams out without any excess loss.*

Introduction

Programmable photonic integrated circuits (PICs) [1] are emerging as versatile chip-scale platforms for applications in many different fields including microwave photonics [2], mode manipulation fiber-optic communications [3] and in free space optics [4], quantum [5] and neural networks [6]. In Silicon photonics (SiP), the possibility of integrating fast and power-efficient tuning elements and on-chip monitor photodetectors enables the realization of photonic processors, which can self-configure to implement specific functionalities [3-4].

In this work, we show that a mesh of Mach-Zehnder Interferometers (MZIs) can automatically self-configure to establish optimal communication channels [7] and recover, without introduction of any excess loss, the information carried by two 10 Gbit/s modulated free-space Hermite-Gaussian beams that are spatially overlapped and share the same wavelength and state of polarization.

Photonic integrated mesh

The SiP circuit consists of a 9×2 diagonal mesh including 15 MZIs (8 MZIs in the first row and 7 MZIs in the second row) arranged as in the scheme of Fig. 1a. The sample (Fig. 1b) was fabricated on a standard 220 nm SiP platform (AMF foundry) by using 500 nm wide channel waveguides. A 3×3 square array of optical antennas (Fig. 1c1), which are labelled as radiation ports (RPs) and implemented though vertically-emitting grating couplers, is used to either couple a free-space optical beam into the photonic chip or to radiate a guided-wave signal out to free space. Each MZIs is thermally tuned by means of TiN heaters (2 µm x 80 µm) to implement an amplitude- and phase-tuneable beam coupler. At the output port of each MZI, transparent CLIPP photodetectors [8] are used to locally monitor the status of each MZI and implement automatic tuning and stabilization procedures (Fig. 1c2). The sample is mounted on an PCB integrating the electronic front-end for the read out of the CLIPP detectors and for providing the control signals to the thermal phase shifters (Fig. 1d). The vertically radiated beams emitted by the grating couplers are steered to horizontal propagation through a turning mirror placed above the sample.

Mode separation and sorting

The mesh of Fig.1 was used to establish and maintain two space-overlapped free-space optical channels with the same wavelength and polarization status. Figure 2a shows the schematic of the setup employed to receive the optical beams from two external sources (fiber collimators) to the mesh (and vice versa). Two bi-convex lenses with the focal length of 50 mm are used in Fourier transforming condition to create the collimated far field of the mesh beam in the plane P1, at the distance of 10 cm from the circuit, and the image plane (plane of the array) at P2. Another bi-convex lens with 75mm focal point creates the collimated far field matched to the aperture of fiber collimators in the center of the cubic beam splitter placed 350mm away from the chip. The beam is then imaged via a 4f system consisting of 250mm bi-convex lens to the fiber collimators.

With this setup, the beam from each source can be individually coupled to the mesh and tracked through the automatic tuning and stabilization of each row of the mesh. This can be done by independent tuning of the MZIs by minimization of the output power at monitor detectors (CLIPP in Fig.1.c2) [3]. The signals from the two sources can be identified by the detectors through using suitable labels (pilot
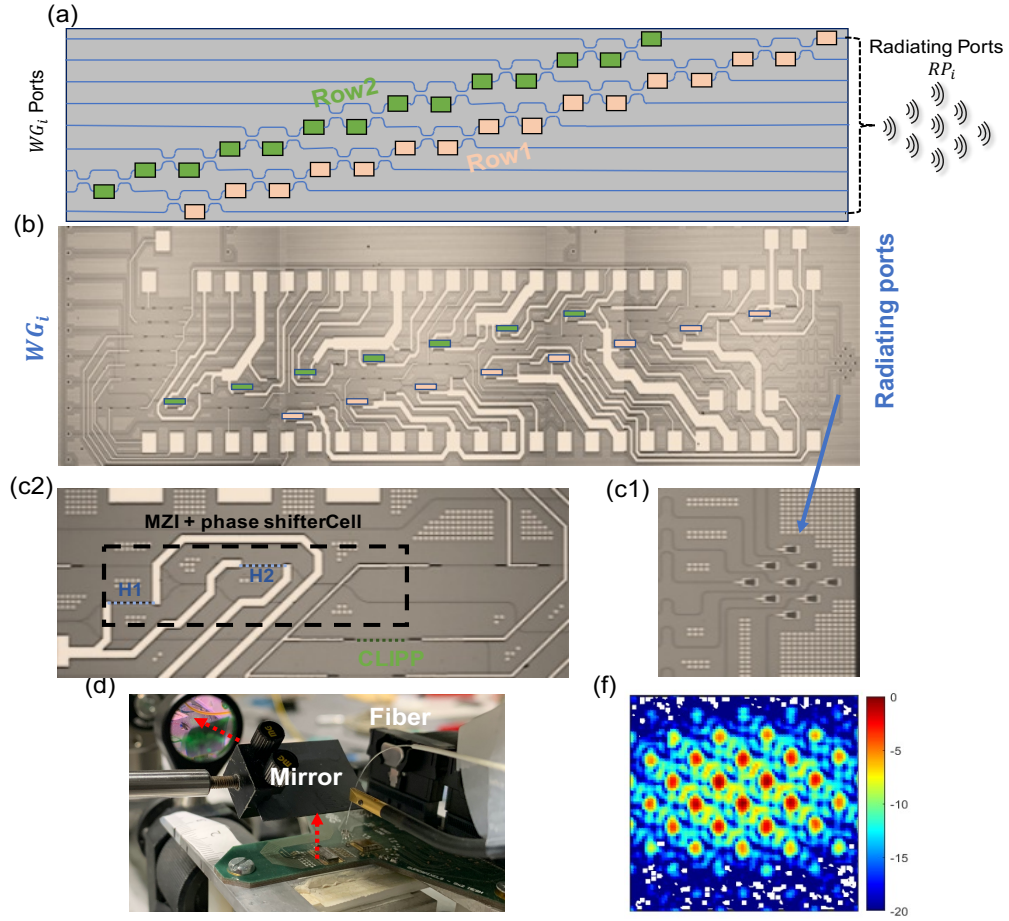
Fig. 1: (a) Schematic of the 9×2 diagonal mesh of MZIs with a pair of phase actuators in each stage (differentiated by colors for different rows of the mesh); (b) Microscopic picture of the fabricated silicon chip highlighting MZI elements of row 1 (yellow boxes) and 2 (green boxes). (c1) Detail of the 3×3 array of grating couplers used as radiation ports and (c2) of the MZI thermally tuneable beam coupler followed by a transparent detector (CLIPP). (d) Experimental the setup showing the fiber coupling to the WGi ports of the mesh and turning mirror. (f) Collimated far field of the array captured with NIR camera when mesh is tuned to couple to a fiber collimator.

tones) superimposed as shallow amplitude modulations on each channel. To understand the working point of the mesh in the tuned configuration, we reversed the direction of the light propagation (launching into WG1 port) while looking at the far field pattern of the mesh (transmitter mode) by a NIR camera focused on the plane P1 after an 8% splitter. The spacing between the RPs of the array (~32λ) leads to the far field pattern which includes several diffraction orders spread closely (1.7 degrees apart) as recorded in Fig.1f. Far field is automatically reconfigured to align the main lobe of the radiation diagram (the one with highest gain) to the position of the collimators for each row of the mesh.

An interesting scenario happens when the beams from the two sources and same diffraction limited channels overlap spatially at the RPs of the mesh, with the same wavelength and state of polarization. Theoretically, if the two channels are spatially orthogonal, they can be still separated. With a pair of conventional spatial light modulators (SLM) this operation can be

performed, yet at the price of a 3dB loss to split the two overlapped beams in two paths. While a 2-diagonal mesh (two rows of MZIs) is enabled of separating the two beams without any excess loss. Using the experimental setup of Fig. 2a, two orthogonal modes are generated by introducing a 0-π phase jump across the beam from one of the sources (collimator II), resulting in the excitation of the higher order 01 Hermite-Gaussian mode (the output of collimator is the fundamental Hermite-Gaussian mode). If the first row of the mesh is configured to maximize the coupling with the fundamental mode at port WG1, the higher order mode suffers 27dB of rejection at the same port. From this state, the mesh can automatically self-configure to couple the higher order mode to port WG1, leading to about 24dB rejection of the fundamental mode. Similar performance is observed simultaneously at port WG2 (output of row 2) for the orthogonal modes.

To examine the capability of the mesh to separate the two orthogonal, yet spatially overlapped beams, two independently modulated 10Gbit/s OOK channels were transmitted on the
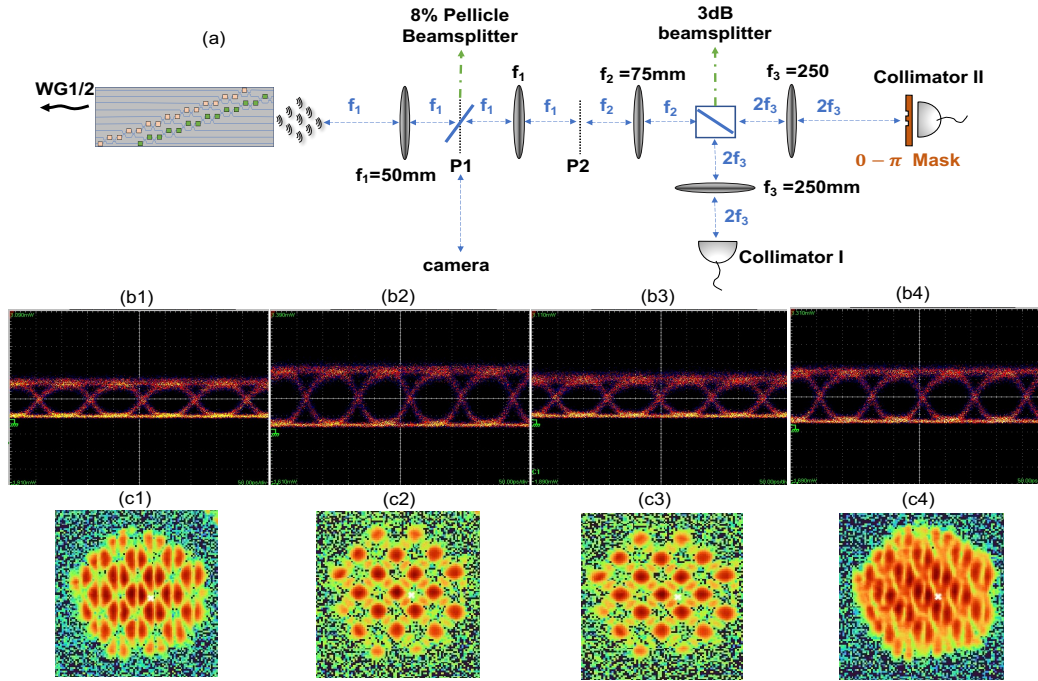
Fig. 2: (a) Schematic of the experimental setup. (b) Eye diagram of 10Gbit/s OOK modulated channel from collimator II to WG1 (b1), Collimator I to WG2 (b2), collimator II to WG2 (b3) and collimator I to WG1 (b4) when mesh is automatically tuned to each of these sources. Far-field radiated by the RPs of the mesh when the direction of the light propagation is reversed (from the mesh to the collimators): (c1) WG1 to higher order mode and (c2) WG2 to fundamental mode; (c3) WG1 to fundamental mode and (c4) WG2 to higher order mode.

fundamental and higher order Hermite-Gaussian mode at the same carrier wavelength (1550 nm) and same polarization state.

By tuning the first and second row of the mesh, the two modes (channels) are separated and arbitrarily sorted out at the output ports WG1 and WG2. As shown by the eye diagram of the recovered signals in Fig.2(b1-b4), negligible residual crosstalk from the interfering orthogonal mode is observed. To get a deeper insight in the operation of the programable mesh, we reverse the direction of the light propagation from the mesh to the external collimators as receivers and we used a NIR camera focused to plane P1 to image the far filed radiated by the RPs. Figure 2(c1) and (c2) shows the far field pattern observed when the mesh is in the state of eye diagrams 2(b1) and 2(b2); shining the light form WG1 and WG2, the far field pattern matches the shape of the higher order mode and the fundamental mode, respectively; by switching the state of the mesh to the state of the eye diagrams 2(b3) and 2(b4), the far field pattern changes to the orthogonal configuration. Noteworthy, the mesh is reconfiguring by simply minimizing the power at each stage of the rows without any prior knowledge of the incoming beams.

Conclusions

We establish two spatially overlapping free space channels sharing the same diffraction limit for two 10 Gbit/s signals using a 9x2 self-configuring SiP mesh without introduction of any excess loss. We demonstrated that mesh can be automatically reconfigured to obtain optimum coupling to incoming beam front. Applications are envisioned to more advanced free-space optical processing, including phase front reconstruction, beaming through scattering media and chip-to-chip free space communications.

References

[1] W. Bogaerts, et al. "Programmable photonic circuits". Nature 586, 207–216 (2020). https://doi.org/10.1038/s41586-020-2764-0

[2] D. Pérez, et al., "Toward Programmable Microwave Photonics Processors," J. Lightwave Technol. 36, 519-532 (2018)

[3] A. Annoni, et al. "Unscrambling light—automatically undoing strong mixing between modes". Light: Science & Applications 6, e17110 (2017).

[4] M. Milanizadeh, et. al. "Automated manipulation of free space optical beams with integrated silicon photonic meshes," arXiv:2104.08174

[5] X. Qiang, et al., "Large-scale silicon quantum photonics implementing arbitrary two-qubit processing," Nat. Photonic, vol. 12, pp. 534–539 (2018)

[6] Y. Shen er al., "Deep learning with coherent nanophotonic circuits," Nat. Photonics, vol. 11, pp, 441–446 (2017)

[7] David A. B. Miller, "Establishing Optimal Wave Communication Channels Automatically," J. Lightwave Technol. 31, 3987-3994 (2013)